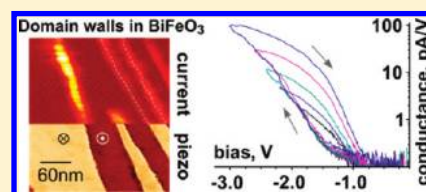


Dynamic Conductivity of Ferroelectric Domain Walls in BiFeO₃Peter Maksymovych,^{*,†,#} Jan Seidel,^{*,‡,§,#} Ying Hao Chu,^{||} Pingping Wu,[⊥] Arthur P. Baddorf,[†] Long-Qing Chen,[⊥] Sergei V. Kalinin,[†] and Ramamoorthy Ramesh^{‡,§}[†]Center for Nanophase Materials Sciences, Oak Ridge National Laboratory, Oak Ridge, Tennessee 37831, United States[#]Materials Sciences Division, Lawrence Berkeley National Laboratory, Berkeley, California 94720, United States[§]Department of Materials Science and Engineering and Department of Physics, University of California, Berkeley, California 94720, United States^{||}Department of Materials Science and Engineering, National Chiao Tung University, Hsin Chu, Taiwan, Republic of China[⊥]Department of Materials Science and Engineering, Pennsylvania State University, University Park, Pennsylvania 16802, United States Supporting Information

ABSTRACT: Topological walls separating domains of continuous polarization, magnetization, and strain in ferroic materials hold promise of novel electronic properties, that are intrinsically localized on the nanoscale and that can be patterned on demand without change of material volume or elemental composition. We have revealed that ferroelectric domain walls in multiferroic BiFeO₃ are inherently dynamic electronic conductors, closely mimicking memristive behavior and contrary to the usual assumption of rigid conductivity. Applied electric field can cause a localized transition between insulating and conducting domain walls, tune domain wall conductance by over an order of magnitude, and create a quasicontinuous spectrum of metastable conductance states. Our measurements identified that subtle and microscopically reversible distortion of the polarization structure at the domain wall is at the origin of the dynamic conductivity. The latter is therefore likely to be a universal property of topological defects in ferroelectric semiconductors.

KEYWORDS: Bismuth ferrite, domain wall, conductivity, ferroelectric, memristive system, pinning



COMMUNICATION

Ferroic materials spontaneously develop macroscopic polarization, magnetization, and strain.¹ Topological defects in the continuous structure of the corresponding order parameters, e.g. domain walls, domain junctions, and vortices,^{2,3} are associated with a change of symmetry, strong field, and strain gradients and can be localized on 1–10 nm length scales in one of the three dimensions.^{1,4} Those topological defects that exhibit nontrivial electronic or magnetic behavior can act as building blocks for nanostructures^{5,6} defined within the continuous physical volume of the material by spatially varying lattice symmetry rather than physical shape or chemical composition. Such topological nanostructuring is mass conserving, allowing nanostructures to be created, erased, and reconfigured within the same physical volume almost indefinitely.

Over the past few years, significant progress has been made in the understanding of the atomic, magnetic,^{7,8} and electronic structure⁹ of domain walls in ferroelectric and multiferroic materials and pathways to control domain morphology via material design¹⁰ and electric fields.³ Intriguingly, topological defects in several material systems were found to possess distinct electronic properties. These include superconducting twin walls in Na-doped WO₃,¹¹ conducting domain walls in BiFeO₃,¹² and insulating antiphase boundaries in YMnO₃.¹³ Understanding the origin of these phenomena is challenging because of a variety of competing or even coexisting scenarios. For example, the origin of electronic conductivity in domain walls in BiFeO₃,

currently under debate, has been attributed to either vacancy aggregation due to an intrinsic electric dipole at the wall¹⁴ or local band gap lowering due to a significant distortion of the rhombohedral symmetry of the BiFeO₃ unit cell at the domain wall.^{9,12,15}

Here we have revealed for the first time that domain walls in BiFeO₃ are not rigid electronic conductors, as considered before, but are in fact intrinsically dynamic conductors. By combining conductive and piezoresponse force microscopies¹⁶ to characterize, respectively, the nanoscale electron transport and polarization dynamics, we have inferred that the applied electric field induces local, microscopically reversible distortions of the domain wall's polarization profile during transport measurements. These distortions dramatically enhance electronic conductance of the domain walls compared to their undistorted, as-grown state, and even more intriguingly make the conductance reproducibly tunable via electric field. The resulting memristive-like behavior is likely to be general to ferroelectric domain walls in semiconducting ferroelectric and multiferroic materials, and it may potentially find uses in multilevel memory functionality, universal logic,¹⁷ adaptive learning,^{18,19} and pattern recognition.²⁰ Furthermore, significant contribution from the intrinsic polarization dynamics necessitates a more in-depth treatment of the electronic conductance in ferroelectric materials, beyond equilibrium structures at zero field.

Received: December 14, 2010

Revised: March 29, 2011

Published: April 12, 2011

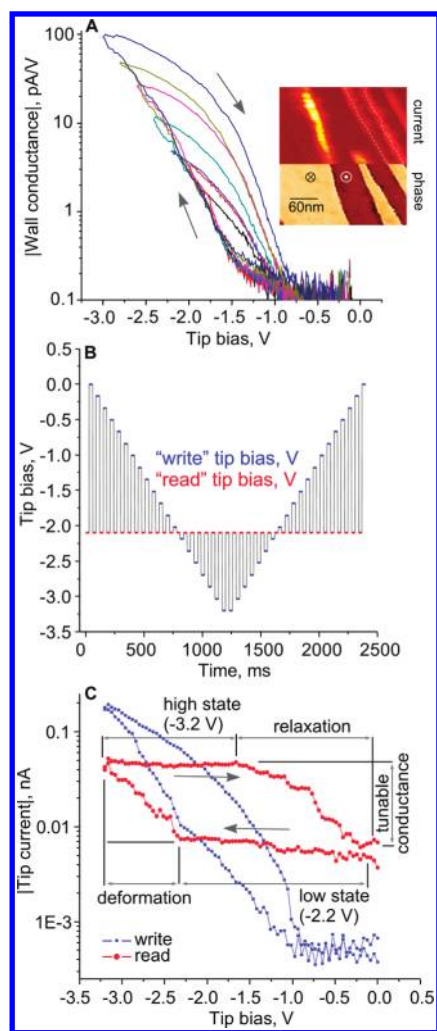


Figure 1. (A) A series of hysteretic I – V curves obtained sequentially on the surface of BiFeO₃ film (postannealed at oxygen pressure of 10^{-4} bar) by increasing peak negative bias after each consecutive I – V curve. The arrows show the direction of the forward (toward increasing negative) and reverse tip bias sweeps. The inset shows microscopic images of piezoresponse phase (bottom half) and current (top half) acquired simultaneously on the surface of a film postannealed at 1 bar of oxygen, with dashed lines marking the center of the 109° domain walls as judged from the phase image. (B) Tip bias waveform used to probe the occurrence, stability, and tunability of quasicontinuous conducting states at the domain walls. (C) The resulting transport blue/red I – V curves represents the “write”/“read” values of tip current acquired at blue/red points in (B).

100 nm thick La-doped (10%) BFO thin films were grown by pulsed laser deposition on DyScO₃/SrTiO₃(001) substrates.¹⁰ Periodic arrays of ferroelectric 109° domain walls, where the change occurs in both in- and out-of-plane components of spontaneous polarization, were created through a systematic control of the growth conditions.¹⁰ Scanning probe microscopy experiments were carried out in a customized ultrahigh-vacuum atomic force microscope (VT STM/AFM, Omicron) using Pt-coated (Mikromasch, CSC37, and Budget sensors, Multi-75). All the measurements were performed at a background pressure of 3×10^{-10} Torr after transferring the sample from ambient without any subsequent treatment. The I – V curves were acquired in the conductive AFM regime, with the tip in contact with the surface

(loading force ~ 1 nN), using a variable-bandwidth current preamplifier (FEMTO DLPCA-200) with a noise floor of ~ 100 fA and applying a linear bias ramp with a rate of 1–5 V/s. Simultaneous piezoresponse force microscopy was carried out by superimposing an AC bias on top of the DC bias for conductive measurements. The AC bias parameters ranged from 100 to 200 mV in magnitude and from 200 kHz to 350 kHz in frequency, chosen for each cantilever to be near its first contact resonance. The total piezoresponse signal corresponds to $A_0 \cdot \sin(\phi)$, where A_0 is the amplitude, and ϕ is the phase of the cantilever oscillation relative to the exciting AC signal.

In agreement with a previous work,¹² the domain walls were reproducibly conducting, Figure 1A and inset. Significant conductivity was observed only at negative tip bias, while little or no current could be measured at the positive tip bias up to ferroelectric switching voltages (which strongly alter and erase domain walls). This asymmetry of conduction with respect to bias polarity is most likely related to the asymmetry of the top (Pt tip–surface) and bottom (SrRuO₃/BiFeO₃) conducting interfaces (e.g., due to the difference in the Schottky barrier height). Upon detailed characterization, we have found that independent of the position along the domain wall or its conductance, local I – V curves exhibited significant hysteresis (Figures 1A and S1, Supporting Information), with current in the reverse direction always significantly exceeding that in the forward direction of the voltage scan. Remarkably, the magnitude of current hysteresis depended on the history of the applied bias, similar to the distinct behavior of memristive systems.²¹ This is seen in Figure 1A, where the area of the hysteretic window depends strongly on the range of tip bias used to acquire the I – V curve. In particular, the I – V curves were similar in the forward voltage scan direction, but they were pinched off at the maximum bias/current value yielding a unique reverse I – V curve for every value of the maximum bias. Therefore, the domain wall is not a rigid conductor, as previously considered. Instead it supports a quasicontinuous progression of distinct conducting states induced by an applied electric field.

The properties of such states were probed using a special bias waveform, Figure 1B, that separates the field-induced change of the system state (judged from conductance) from the field dependence of electronic conductivity. An example of such a measurement is shown in Figure 1C, where cycling the tip bias between 0 and -3.2 V revealed a hysteresis of conductance (measured at -2.2 V), with constant low and high conductance states and quasicontinuous transitions in between. Notably, the conductance state created at -3.2 V was *stable* down to -1.7 V and began to gradually relax between -1.7 and 0 V. The tunability and relative stability of the conductance states enables a prototypical multilevel storage functionality at each single location along the domain wall. Figure 2A demonstrates four distinct conductance states created by progressively increasing the “write” bias from -3.2 to -4 V and by applying -2.2 V to “read-out” the conductance state. The distinct conductance states were found to be stable on the time scales up to several minutes (Figure 2B), with relaxation being more pronounced for more conducting states. The relaxation threshold was ~ -1.2 V for all the recording bias values (Figure 1C). While this prevents nonvolatile memory function at present, the built-in electric field and the respective relaxation rate can prospectively be tuned through the choice of the electrostatic boundary conditions,^{22,23} and the relaxation behavior will furthermore depend on the type of the topological defect.

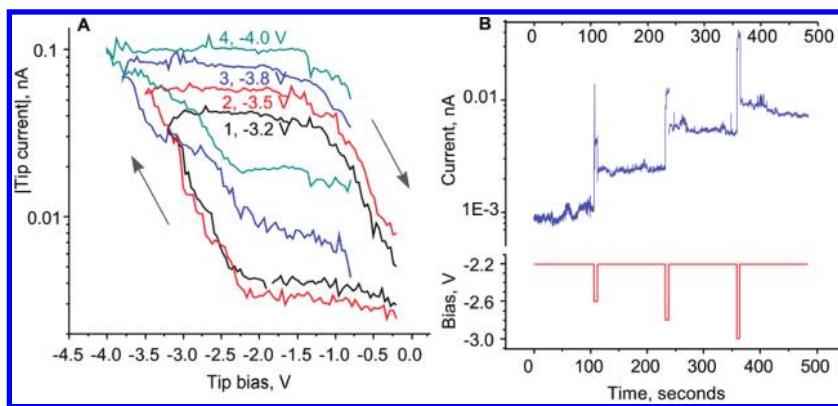


Figure 2. (A) A sequence of current hystereses acquired at a single location on the domain wall by repeating the measurement in Figure 1B and C as a function of increasing peak write bias. The gray arrows mark the direction of the bias ramp. (B) Three levels of conductance created consecutively by bias pulses of -2.6 , -2.8 , and -3.0 V and monitored at -2.2 V for 4 min each.

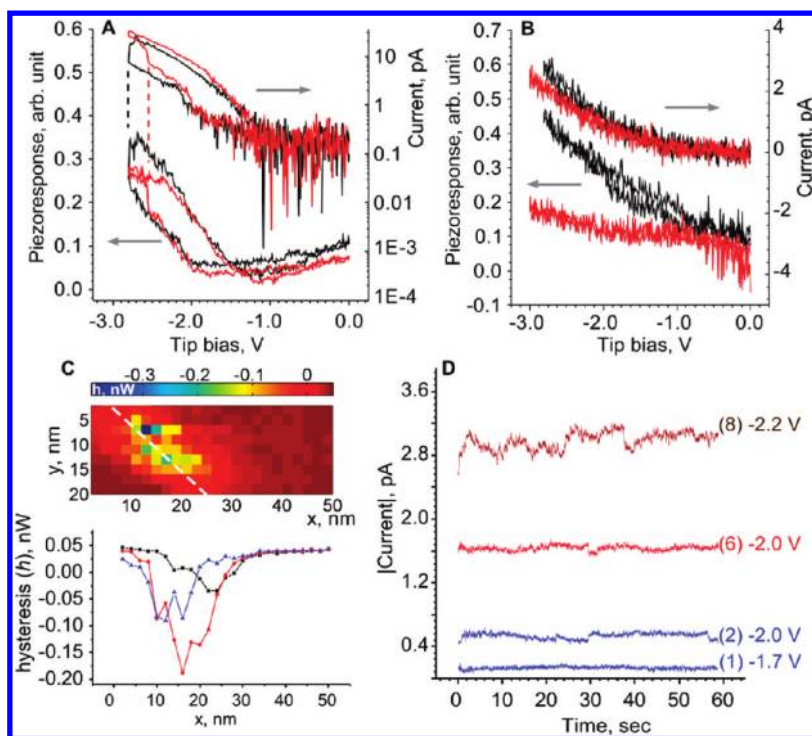


Figure 3. (A and B) Simultaneous measurements of local piezoresponse and conductance as a function of tip bias. Each graph shows current (top) and total piezoresponse signal (bottom) acquired on two locations (red and black) along the domain wall (A) and on the domain face (B). (C) Map of hysteresis, h , (calculated as the area under the hysteretic $I-V$ curve) across the domain wall, obtained by repeated acquisition of the $I-V$ curves as the tip was systematically displaced toward and across the domain wall. The white dashed line is the approximate location of the domain wall center. Bottom panel shows several slices of the map along the x -direction. (D) Time dependence of current at a single location on the domain wall as a function of tip bias.

An applied electric field can drive a variety of processes at the domain wall, both intrinsic, such as a locally distorted polarization structure, and extrinsic, such as charge injection and motion of oxygen vacancies. We have employed simultaneous measurement of local conductivity and converse piezoresponse¹⁶ to probe the local polarization structure, utilizing the fact that the sign and the magnitude of piezoresponse is proportional to the sign and the magnitude of spontaneous polarization.²⁴ As seen, in Figure 3A, significant and characteristic piezoresponse hysteresis coexisted with the hysteresis in the $I-V$ curve. The overall shape of the two hystereses is markedly similar, both in the absolute size

of the hysteresis window and the bias values where both values increased abruptly (dashed lines in Figure 3A). The latter events identify abrupt changes in the polarization configuration, akin to Barkhausen jumps²⁵ in domain wall motion. At the same time, neither conductance nor piezoresponse were significantly hysteretic away from the domain walls (Figure 3B), within the same range of tip bias and polarity. These measurements strongly argue that the origin of the observed hysteresis is a localized polarization distortion at the domain wall that is both microscopically reversible and stable within a certain range of tip bias, as inferred from Figure 1C. The stability of the distorted state in a

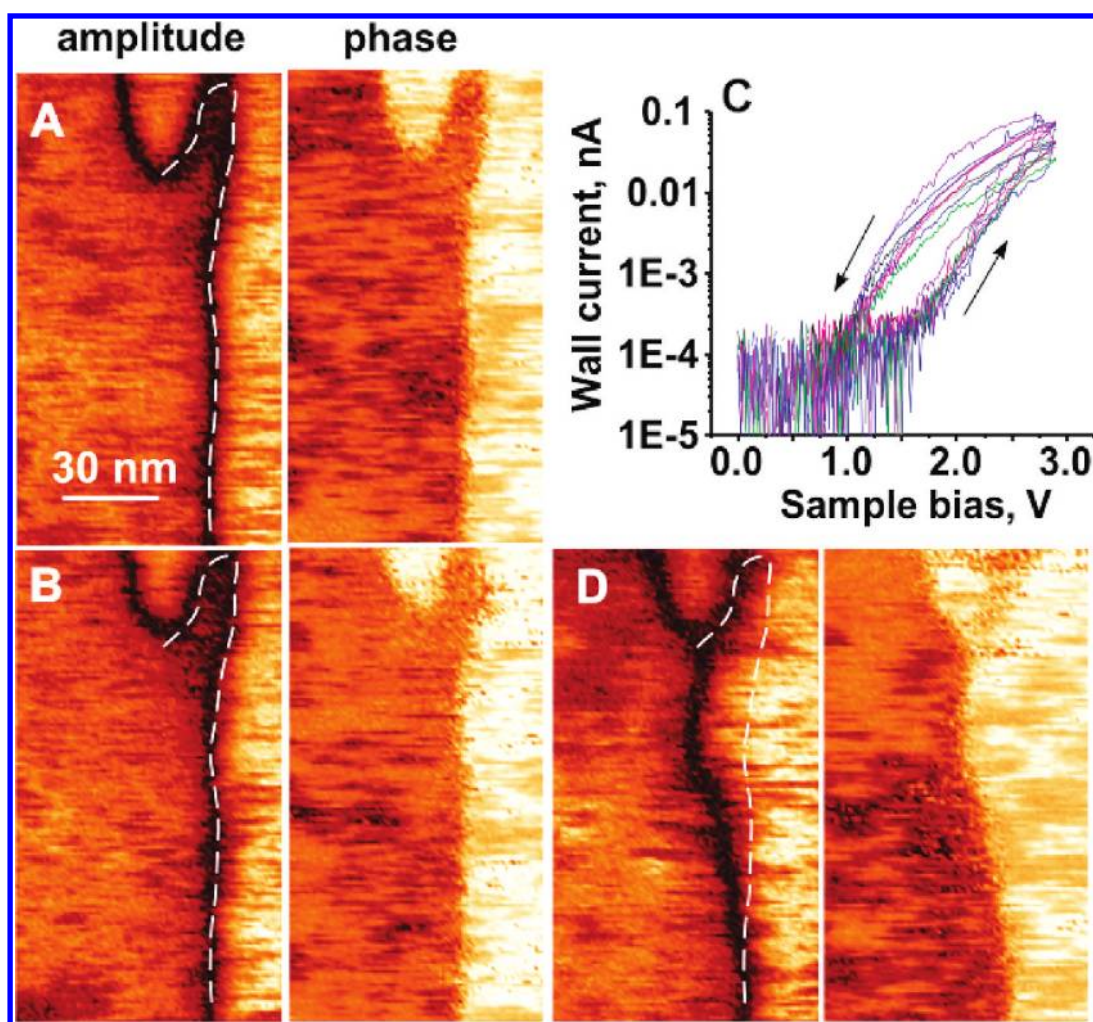


Figure 4. Evolution of the domain wall profile along the surface when it is subject to conductive measurements. (A) PFM image (amplitude and phase) of the 109° domain wall before I – V curve acquisition. (B) PFM image acquired after measuring 10 I – V curves (shown in C) along the domain wall with a maximum tip bias of -2.9 V. (D) PFM image after subjecting the wall to several pulses of -3.2 V. White dashed line is an approximate profile of the undistorted wall from (A) and (B).

relatively broad range of electric fields (Figure 1) arises from the pinning of the distorted polarization configuration, for example, by wall–defect²⁶ or wall–lattice (Peierls potential)²⁷ interactions. At the same time, the complete relaxation (within the limits of our measurements) of the distorted state after the electric field is turned off can be witnessed from the conductance hysteresis in Figure 1C and the piezoresponse hysteresis in Figures 3A and 4A–C, where PFM images of the domain wall before (Figure 4A) and after (Figure 4B) acquisition of the I – V curves (Figure 4C) are shown. Clearly, the domain walls in Figure 4A and B are indistinguishable within the resolution of our PFM measurement (~ 8 nm) after as many as 10 hysteretic I – V curves. If the tip bias exceeded ~ -3.2 V, then the domain wall however would begin to visibly displace, as shown in Figure 4D, as expected. The I – V curves in this case remained hysteretic, and the conductance was still tunable (as seen in Figure 2A), provided the displacement was not much larger than the area of the tip–surface junction. Parenthetically, both reversible and irreversible distortions have recently been detected on a local scale in LiNbO_3 ,²⁸ lead zirconate,²⁹ and bismuth ferrite,³ adding evidence that this behavior is general for ferroelectrics.

In principle, the conductance hysteresis at the domain wall can arise if the domain wall were a nonhysteretic conductor, but the wall location within the tip–surface contact region would be changed by the electric field. As in any ferroelectric, a negatively biased tip will displace the wall in a direction that increases the area of the upward polarized domain, which we confirmed directly (Figure S2, Supporting Information). Therefore, in this simple scenario, domain wall displacement would increase the conductance of the reverse I – V curve on one side of the wall and decrease it on the other. In contrast, the measured conductance is *always* higher on the reverse branch of the I – V curve, on either side of the domain wall (Figure 3C). Another possible source of hysteresis accompanying ferroelectric dynamics is the displacement current due to rearrangement of bound polarization charges. This scenario can be ruled out by observing weak time dependence of the domain wall current, Figure 3D, where the domain wall conductance was negligibly time dependent for a duration of 1 min. Negligible time dependence of current also argues strongly against ionic motion, e.g., field-induced migration of oxygen vacancies, as a primary source of the observed hysteresis and is in stark contrast to the strongly time-dependent conductivity of Ca-doped BiFeO_3 films, where ionic conductivity was implicated.³⁰

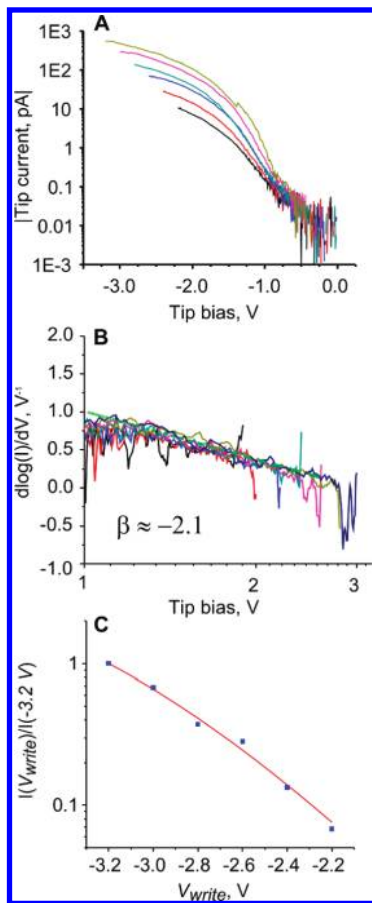


Figure 5. (A) Bias dependence of current-normalized differential conductance obtained from reverse I – V curves in Figure 4A. (B) Exponent β ($d \log(I)/dV \propto V^{-\beta}$) was obtained from a least-squares fit (green line) to the reverse curve with maximum conductance. (C) Domain wall current at $U = -2$ V as a function of peak bias in the I – V curve extracted from Figure 4A, normalized to the maximum value at the peak bias of -3.2 V. The red line is a fit for the change of the barrier height in the FN tunneling mechanism, assuming a 1D electrostatic potential of a disk with radius 5 nm and dielectric anisotropy of 0.9 and a linear decrease of the barrier height with increasing peak bias (see text).

The nontrivial effect of polarization distortion of the domain wall on the electronic structure of BiFeO₃ may have several origins. In BiFeO₃, polarization vectors are aligned with the $\langle 111 \rangle$ crystallographic directions, allowing eight possible orientations in the (100) oriented film and three trajectories of polarization switching by 71°, 109°, and 180° degrees.^{3,31} When occurring on the local scale, the distortion of the equilibrium configuration of the 109° domain wall will give rise to significant changes of local electrostatics due to either depolarizing fields or formation of charged head-to-head (tail-to-tail) domain junctions. The occurrence of such junctions is anticipated based on symmetry arguments and was predicted by first-principles analysis of domain-wall motion in PbTiO₃³² and analytical theory of 180° domain walls³³ as well as phase-field modeling of local ferroelectric switching on the BiFeO₃ surface.³ Perturbation in local electrostatics associated with charged junctions will translate into electronic conductance, e.g., through a change in the shape or height of the potential barrier at the tip–surface junction, local accumulation of local compensating charges, or interaction with charged defects (such as oxygen vacancies)³⁴ or a combination of

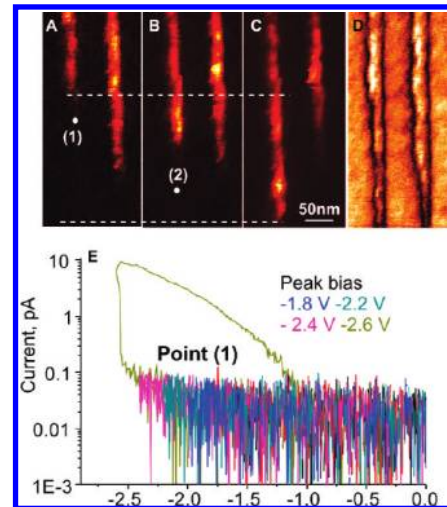


Figure 6. (A–C) A sequence of three current images of the domain walls obtained: (A) before voltage stressing, (B) after acquiring a series of I – V curves (E) at location (1), and (C) after acquiring a similar series of I – V curves (Supporting Information) at location (2). The white dashed lines mark the initial region of the left domain wall, below which the conduction was activated as a result of voltage stressing. (D) Piezoresponse amplitude image of the domain walls in A–C, obtained after (C).

the above. There also exists a possibility that the dynamic polarization distortion further reduces the band gap BiFeO₃ compared to the as-grown configuration. For the latter, reduction of the gap due to local symmetry change was theoretically predicted.⁹

We have shown earlier that local I – V curves from wide band gap semiconductors can be efficiently analyzed by evaluating the bias dependence of current-normalized differential conductance $d \log(I)/dV$.³⁵ When applied to reverse I – V curves (Figure 5A), this analysis reveals that $d \log(I)/dV \propto V^{-2 \pm 0.3}$ (Figure 5B). Under the assumption of the 1D transport geometry, this relatively high exponent in V implies Fowler–Nordheim (FN) tunneling³⁶ as the dominant transport mechanism, for which

$$\frac{d \log I}{dE} = \frac{2}{E} + \frac{8\pi\sqrt{2}m_{\text{eff}}e}{3h} \frac{\phi_B^{3/2}}{E^2}$$

where E is the electric field across the triangular-shaped tunneling barrier, m_{eff} is the effective mass of a tunneling electron, and ϕ_B is the interfacial barrier height. As seen in Figure 4C, the domain wall current (at a tip bias of -2 V in Figure 5A) grows approximately exponentially with the maximum value of the probed tip bias (V_{write} , cf. Figure 1b), increasing by about a factor of 15 when V_{write} is increased from -2.2 and -3.2 V peak bias. We assumed that the major difference between the I – V curves stems from the change of the barrier height (ϕ_B), rather than the variation in the built-in field or the effective area of the transport junction, and that barrier height varies linearly with the “write” bias $\phi(V_{\text{write}}) = \phi_0(1 - \alpha V_{\text{write}})$. Then the relative change of the tunneling current can be estimated from the FN equation as

$$\frac{I(V_{\text{set}})}{I(V_{\text{max}})} = (1 - \alpha V_{\text{set}}) \exp\left(-\frac{8\pi\sqrt{2}m_{\text{eff}}}{3h} \frac{\phi_0^{1.5}}{E_{\text{eff}}} ((1 - \alpha V_{\text{set}}) - 1)\right)$$

We chose $I(V_{\text{max}})$ to be the highest conducting state ($V_{\text{write}} = -3.2$ V) and assumed a simple disk model to relate applied

potential to the electric field of the tip.¹⁶ Despite the large number of unknown material and tip parameters (most importantly the barrier height and electric field strength), we have found that the experimental values can be satisfactorily fit with $\alpha \sim 0.8$. For $\phi_0 = 0.2$ eV and disk radius ~ 5 nm (fit shown in Figure 5C), the total barrier change across a series of I – V curves in Figure 5A would therefore be $\Delta\phi = 0.15$ eV between the most and the least conducting states. The highly nonlinear tunneling mechanism amplifies such relatively small barrier changes into the observed order-of-magnitude tunability of conductance in the narrow range of “write” voltage.

The ultimate manifestation of polarization tunable domain wall conductance is a bias-induced transition between nonconducting and conductive domain wall states. We have frequently observed that as-grown domain walls do not appear conductive, as for example in Figure 6A, where the conductive trace along the wall terminates abruptly. However, applying bias over a certain threshold can activate the conductivity. A sequence of I – V curves in Figure 6E was acquired at position (1) in Figure 5A, incrementing the tip bias by -0.2 V after each curve. Upon reaching -2.6 V, an abrupt event caused the conductance to increase by almost 2 orders of magnitude (Figure 5E, green). The abruptness of this event is closely reminiscent of polarization-induced resistive switching on the surface of ferroelectric lead–zirconate titanate.¹⁶ A rescan of the same area (Figure 6B) reveals that ~ 80 nm along the wall of the previously nonconducting wall became conducting similarly to adjacent segments, with the rest of the area still remaining insulating. Repeating the activation experiment in the adjacent domain wall region yielded a comparable result (Figure 6C), with a similarly abrupt onset (Figure S3, Supporting Information). The activation has therefore a pronounced non-local character and can be rationalized as an electric-field-induced depinning^{26,37} of the domain wall from a strongly pinned, as-grown, and poorly conducting configuration into a weakly pinned conducting configuration.

In summary, the domain walls in BiFeO₃ were found to be inherently dynamic conductors due to a product of three factors: (1) electric-field-induced distortion of the polarization structure at the domain wall; (2) the dependence of conductivity on the degree of distortion; (3) weak pinning of the distorted wall, manifested as the stability of the distorted configuration in a relatively broad voltage window. The domain wall is thus not a rigid electronic conductor, instead offering a quasicontinuous spectrum of voltage tunable electronic states. This is different from the interior of ferroelectric domains, where switching is anticipated to give rise to discrete and often only two conductance levels.³⁸ The intrinsic dynamics of domain walls and other topological defects in the applied electric field should influence future theoretical and experimental interpretations of the electronic phenomena associated with topological defects in ferroic materials. On the other hand, electron transport appears to be a highly sensitive probe of these dynamics and may be used to probe unique multiferroic properties of ferroelectric domain walls, e.g., magnetization within the antiferromagnetic matrix³⁹ due to order parameter coupling and localized secondary order parameters.⁵ Of obvious future interest is what sets the limits to such transport behavior: Can one “engineer” the topological structure of the domain wall to controllably induce electronic phase transitions within the wall arising from correlated electron nature of BiFeO₃⁴⁰ and charge-ordered multiferroics?⁴¹

■ ASSOCIATED CONTENT

S Supporting Information. Supporting Information contains additional I – V spectra and domain wall images (PFM and cAFM) that reveal: the effect of post-annealing on conductivity of BiFeO₃ films, long-term domain wall creep driven by a biased tip, conductive hot-spots along the domain wall and the onset of polarization distortion as estimated from the slopes of the I – V curves. This material is available free of charge via the Internet at <http://pubs.acs.org>.

■ AUTHOR INFORMATION

Corresponding Author

*E-mail: maksymovychp@ornl.gov; jseidel@berkeley.edu.

Author Contributions

#These authors contributed equally.

■ ACKNOWLEDGMENT

Experiments were performed at the Center for Nanophase Materials Sciences, which is sponsored at the Oak Ridge National Laboratory by the Office of Basic Energy Sciences, U.S. Department of Energy. The work at Berkeley is partially supported by the SRC-NRI-WINS program as well as by the Director, Office of Science, Office of Basic Energy Sciences, Materials Sciences Division of the U.S. Department of Energy under contract no. DE-AC02-05CH1123. J.S. acknowledges support from the Alexander von Humboldt Foundation.

■ REFERENCES

- (1) Rabe, K. M.; Ahn, C.-H.; Triscone, J.-M. *Physics of Ferroelectrics: A Modern Perspective*; Springer: Berlin, Germany, 2007; p 390.
- (2) Naumov, I. I.; Bellaiche, L.; Fu, H. *Nature* **2004**, *432*, 737–740.
- (3) Balke, N.; Choudhury, S.; Jesse, S.; Huijben, M.; Chu, Y. H.; Baddorf, A. P.; Chen, L. Q.; Ramesh, R.; Kalinin, S. V. *Nat. Nanotechnol.* **2009**, *4*, 868–875.
- (4) Salje, E. K. H. *ChemPhysChem* **2010**, *11*, 940–950.
- (5) Salje, E.; Zhang, H. *Phase Transitions* **2009**, *82*, 452–469.
- (6) Allwood, D. A.; Xiong, G.; Cowburn, R. P. *J. Appl. Phys.* **2006**, *100*, 123908.
- (7) Goltsev, A.; Pisarev, R.; Lottermoser, T.; Fiebig, M. *Phys. Rev. Lett.* **2003**, *90*, 177204.
- (8) Ueland, B. G.; Lynn, J. W.; Laver, M.; Choi, Y. J.; Cheong, S.-W. *Phys. Rev. Lett.* **2010**, *104*, 147204.
- (9) Lubk, A.; Gemming, S.; Spaldin, N. *Phys. Rev. B* **2009**, *80*, 104110.
- (10) Chu, Y.-H.; He, Q.; Yang, C.-H.; Yu, P.; Martin, L. W.; Shafer, P.; Ramesh, R. *Nano Lett.* **2009**, *9*, 1726–1730.
- (11) Aird, A.; Salje, E. K. H. *J. Phys.: Condens. Matter* **1998**, *10*, L377–L380.
- (12) Seidel, J.; Martin, L. W.; He, Q.; Zhan, Q.; Chu, Y.-H.; Rother, A.; Hawkrigde, M. E.; Maksymovych, P.; Yu, P.; Gajek, M.; Balke, N.; Kalinin, S. V.; Gemming, S.; Wang, F.; Catalan, G.; Scott, J. F.; Spaldin, N. A.; Orenstein, J.; Ramesh, R. *Nat. Mater.* **2009**, *8*, 229–234.
- (13) Choi, T.; Horibe, Y.; Yi, H. T.; Choi, Y. J.; Wu, W.; Cheong, S.-W. *Nat. Mater.* **2010**, *9*, 253–258.
- (14) Xiao, Y.; Shenoy, V.; Bhattacharya, K. *Phys. Rev. Lett.* **2005**, *95*, 247603.
- (15) Seidel, J.; Maksymovych, P.; Batra, Y.; Katan, A.; Yang, S.-Y.; He, Q.; Baddorf, A.; Kalinin, S.; Yang, C.-H.; Yang, J.-C.; Chu, Y.-H.; Salje, E.; Wormeester, H.; Salmeron, M.; Ramesh, R. *Phys. Rev. Lett.* **2010**, *105*, 197603.

- (16) Maksymovych, P.; Jesse, S.; Yu, P.; Ramesh, R.; Baddorf, A. P.; Kalinin, S. V. *Science* **2009**, *324*, 1421–1425.
- (17) Borghetti, J.; Snider, G. S.; Kuekes, P. J.; Yang, J. J.; Stewart, D. R.; Williams, R. S. *Nature* **2010**, *464*, 873–876.
- (18) Jo, S. H.; Chang, T.; Ebong, I.; Bhadviya, B. B.; Mazumder, P.; Lu, W. *Nano Lett.* **2010**, *10*, 1297–1301.
- (19) Pershin, Y.; La Fontaine, S.; Di Ventra, M. *Phys. Rev. E* **2009**, *80*, 021926.
- (20) Mouttet, B. arXiv:1004.0041. Published online: April 1, 2011.
- (21) Di Ventra, M.; Pershin, Y. V.; Chua, L. O. *Proc. IEEE* **2009**, *97*, 1717–1724.
- (22) Chen, F.; Tan, X.; Huang, Z.; Xuan, X.; Wu, W. *Appl. Phys. Lett.* **2010**, *96*, 262902.
- (23) Maksymovych, P.; Balke, N.; Jesse, S.; Huijben, M.; Ramesh, R.; Baddorf, A. P.; Kalinin, S. V. *J. Mater. Sci.* **2009**, *44*, 5095.
- (24) Kalinin, S.; Bonnell, D. *Phys. Rev. B* **2002**, *65*, 125408.
- (25) Lines, M. E.; Glass, A. M. Principles and applications of ferroelectrics and related materials. Clarendon: Oxford, 1977.
- (26) Gopalan, V.; Dierolf, V.; Scrymgeour, D. A. *Annu. Rev. Mater. Res.* **2007**, *37*, 449–489.
- (27) Ma, H.; Kim, W.-J.; Horwitz, J.; Kirchoefer, S.; Levy, J. *Phys. Rev. Lett.* **2003**, *91*, 217601.
- (28) Aravind, V. R.; Morozovska, A. N.; Bhattacharyya, S.; Lee, D.; Jesse, S.; Grinberg, I.; Li, Y. L.; Choudhury, S.; Wu, P.; Seal, K.; Rappe, A. M.; Svechnikov, S. V.; Eliseev, E. A.; Phillpot, S. R.; Chen, L. Q.; Gopalan, V.; Kalinin, S. V. *Phys. Rev. B* **2010**, *82*, 024111.
- (29) Anbusathaiah, V.; Jesse, S.; Arredondo, M. A.; Kartawidjaja, F. C.; Ovchinnikov, O. S.; Wang, J.; Kalinin, S. V.; Nagarajan, V. *Acta Mater.* **2010**, *58*, 5316–5325.
- (30) Yang, C.-H.; Seidel, J.; Kim, S. Y.; Rossen, P. B.; Yu, P.; Gajek, M.; Chu, Y. H.; Martin, L. W.; Holcomb, M. B.; He, Q.; Maksymovych, P.; Balke, N.; Kalinin, S. V.; Baddorf, A. P.; Basu, S. R.; Scullin, M. L.; Ramesh, R. *Nat. Mater.* **2009**, *8*, 485–493.
- (31) Baek, S. H.; Jang, H. W.; Folkman, C. M.; Li, Y. L.; Winchester, B.; Zhang, J. X.; He, Q.; Chu, Y. H.; Nelson, C. T.; Rzchowski, M. S.; Pan, X. Q.; Ramesh, R.; Chen, L. Q.; Eom, C. B. *Nat. Mater.* **2010**, *9*, 309–314.
- (32) Shin, Y.-H.; Grinberg, I.; Chen, I.-W.; Rappe, A. M. *Nature* **2007**, *449*, 881–884.
- (33) Burtsev, E. V.; Chervonobrodov, S. P. *Ferroelectrics* **1982**, *45*, 97.
- (34) He, L.; Vanderbilt, D. *Phys. Rev. B* **2003**, *68*, 134103(1–7).
- (35) Maksymovych, P.; Pan, M.; Yu, P.; Ramesh, R.; Baddorf, A. P.; Kalinin, S. V. *Nanotechnology* **2010**, in review.
- (36) Sze, S. M. *Physics of Semiconductor Devices*; Wiley-Interscience: Hoboken, NJ, 1981; p 880.
- (37) Jo, J.; Yang, S.; Kim, T.; Lee, H.; Yoon, J.-G.; Park, S.; Jo, Y.; Jung, M.; Noh, T. *Phys. Rev. Lett.* **2009**, *102*, 045701.
- (38) Tsymbal, E. Y.; Kohlstedt, H. *Science* **2006**, *313*, 181–183.
- (39) Daraktchiev, M.; Catalan, G.; Scott, J. *Phys. Rev. B* **2010**, *81*, 224118.
- (40) Catalan, G.; Scott, J. F. *Adv. Mater.* **2009**, *21*, 2463–2485.
- (41) Efremov, D. V.; Brink, J.; van den; Khomskii, D. I. *Nat. Mater.* **2004**, *3*, 853–856.